

A multi-channel approach to the study of the $^{18}\text{O}+^{48}\text{Ti}$ reaction within the NUMEN project

ONOUFRIOS SGOUROS(*) on behalf of the NUMEN COLLABORATION

INFN, Laboratori Nazionali del Sud - Catania, Italy

received 7 February 2022

Summary. — The study of the multi-nucleon transfer as competitive processes to the double charge exchange channel has a prominent position among the goals of the NUMEN project. Understanding the degree of competition between successive nucleon transfer and double charge exchange reactions is imperative for the description of the direct-meson exchange mechanism. Moreover, the study of these competing processes under the same experimental conditions provides the appropriate constraints in the experimental systematics that are particularly useful for the theoretical description of the reaction mechanism. To this extent, one- and two-nucleon transfer reactions in the $^{18}\text{O}+^{48}\text{Ti}$ collision at 275 MeV were measured for the first time, under the NUMEN and NURE experimental campaigns. Differential cross-section angular distribution measurements for the reaction ejectiles were performed by using the MAGNEX large acceptance magnetic spectrometer at INFN-LNS in Catania. Recent results for the one-nucleon and two-proton transfer reactions will be presented and discussed.

1. – Introduction

The interest of the physics community for the neutrinoless double beta ($0\nu\beta\beta$) decay is still vivid. Although this process has not been observed yet, several ongoing experiments are seeking evidence for such a rare decay [1-5]. The NUMEN (NUclear Matrix Elements for Neutrinoless double beta decay) project [6, 7] at the Istituto Nazionale di Fisica Nucleare - Laboratori Nazionali del Sud (INFN-LNS) in Catania aims at accessing information relative to the nuclear matrix elements (NMEs) of the $0\nu\beta\beta$ decay by studying double charge exchange (DCE) reactions induced by heavy ions for a variety of $0\nu\beta\beta$ decay candidate targets. Into this context, the ^{48}Ti nucleus is of great interest since it is the daughter nucleus of ^{48}Ca in the $0\nu\beta\beta$ decay process [8, 9]. The use of DCE reactions as probes for studying the $0\nu\beta\beta$ decay stems from the fact that, despite some differences, the two processes have some features in common. Among them, both processes probe

(*) E-mail: onoufrios.sgouros@lns.infn.it

the same initial and final-state nuclear wave functions [6, 10, 11] and moreover, $0\nu\beta\beta$ and DCE matrix elements seem to be in linear correlation [10, 12].

The direct meson exchange mechanism, named also *Majorana* mechanism [11] in analogy to the $0\nu\beta\beta$ process proposed by Ettore Majorana, is only a part of the complete DCE mechanism. Other competitive processes like sequential (multi)nucleon transfer reactions [13], double single charge exchange (DSCE) or a combination between them may provide an important contribution to the final DCE cross-section. In a relevant work, it was demonstrated that experimental data on the ($^{18}\text{O}, ^{18}\text{F}$) reaction are very important to constrain the DSCE mechanism [14]. Moreover, a recent theoretical study [15] for the $^{18}\text{O} + ^{40}\text{Ca}$ reaction at 15 AMeV suggested the combination of single charge exchange (SCE) with sequential one-proton and one-neutron transfer reactions as a second process in the leading order in the $^{18}\text{O} \rightarrow ^{18}\text{Ne}$ transition. So, it is evident that besides the DCE direct channel [16, 17], measurements for all the competitive processes that may contribute to the final DCE cross-section are imperative [18-21].

Direct transfer reactions are excellent spectroscopic tools due to their high selectivity in probing specific degrees of freedom in the populated nuclear states. One-nucleon transfer reactions probe single-particle configurations, while two-nucleon transfer ones offer an insight into pairing correlations [22]. The description of the transfer reaction cross-sections relies on the use of the appropriate reaction model like the one-step distorted-wave Born approximation (DWBA) [23] or more realistic models like the coupled-channels Born approximation (CCBA) [24]. In either case, the basic ingredients for such calculations fall under two main headings: the optical potentials (OPs) that describe the elastic scattering at the entrance and exit channels and the overlap functions (OFs) that contain information on the nuclear structure of the involved nuclei. The OFs are usually determined as single particle solutions of a Woods-Saxon potential multiplied by the corresponding spectroscopic amplitude which is usually derived from large-scale shell model calculations. As regards the OPs, the elastic scattering problem is under control by adopting double-folding potentials like the São Paulo Potential (SPP) [25]. However, measurements on elastic scattering are necessary in order to confirm the validity of the adopted potential [26-28]. The importance of the dependence of the predictions from the models was highlighted in a recent publication of the NUMEN collaboration [18].

Starting from the above considerations, a global study for the complete net of reactions channels involved in the $^{18}\text{O} + ^{48}\text{Ti}$ reaction at 275 MeV was performed as part of the NUMEN and NURE (NUclear REactions for neutrinoless double beta decay) [29] projects. As an example of this multi-channel approach, the present work provides an overview on the data reduction for the one-neutron, one-proton and two-proton transfer reactions. The analysis of the one-proton transfer channel was recently completed and the results are reported in ref. [30], while preliminary results on the analyses of one-neutron and two-proton transfer channels are presented here for the first time. Details on the status of the analysis of the elastic scattering for the $^{18}\text{O} + ^{48}\text{Ti}$ reaction can be found in [31].

2. – Experimental setup

The relevant experiment was performed at INFN-LNS in Catania. The $^{18}\text{O}^{8+}$ ion beam was accelerated by the K800 Superconducting Cyclotron at 275 MeV and impinged on a $510\text{ }\mu\text{g}/\text{cm}^2$ thick TiO_2 target with an aluminum backing. Measurements using a WO_3 target ($284\text{ }\mu\text{g}/\text{cm}^2$) evaporated on an aluminum foil and a $226\text{ }\mu\text{g}/\text{cm}^2$ thick ^{27}Al one were repeated under the same experimental conditions in order to estimate

the background arising from the different target components. The beam spot size at the target position was limited to ≈ 3 mm by means of a collimation system, consisting of a 2 mm diameter collimator followed by a 4 mm diameter anti-scattering, which was mounted upstream the target position.

The various reaction ejectiles were momentum analyzed by the MAGNEX large acceptance magnetic spectrometer [32]. MAGNEX consists of a large aperture quadrupole lens, focusing charged particles along the vertical direction, followed by a large bending magnet (*i.e.*, the dipole) providing focusing strength in the horizontal direction. It is a high-performance optical device which can detect from very light nuclei [33] up to heavy ones [34,35]. In the present setup, the spectrometer optical axis was set at $\theta_{opt} = 9^\circ$ with respect to the beam direction, thus spanning an angular range between 3° and 15° in the laboratory reference frame. The final phase space parameters of the ions trajectories, namely horizontal and vertical positions and incident angles were measured by the Focal Plane Detector (FPD) [36] which is located 1.91 m downstream the exit of the bending magnet. The FPD is a two-stage detector composed of a gas tracker followed by a wall of 60 silicon detectors. The gas tracker is divided into six sections, each one serving as a proportional drift chamber providing the energy loss signal (ΔE) of the ions inside the gas and as a position-sensitive proportional counter for the measurement of the horizontal and vertical positions of the ions track, thus allowing the determination of the corresponding horizontal and vertical angles, respectively. In this way, the reconstruction of the ions track may be performed. Finally, the ions residual energy E_{resid} is measured by the silicon wall where the ions stop. Moreover, the FPD was also used in order to discriminate the ions of interest among the various reaction products, by means of the conventional ΔE - E method for the Z separation and a technique for the determination of the mass number based on the correlation between the ions kinetic energy and the measured horizontal position at the focal plane. The main features of the particle identification pertinent to this work are presented herewith, while an extensive description is reported in ref. [37]. As a representative case, the identification process for the events corresponding to the one-neutron stripping reaction is illustrated in fig. 1. A similar procedure was also adopted for the identification of all other reaction channels involved in the $^{18}\text{O} + ^{48}\text{Ti}$ collision.

3. – Data reduction

Once the reaction channel of interest is identified, a high-order software ray reconstruction technique [38] is applied to the data and the momentum vector of the ions at the target position is deduced. In what follows, a brief description of the ray reconstruction technique is presented.

For an accurate reconstruction of the ions trajectories, a precise model for the spectrometer response is imperative. The basic ingredient of this model is called direct transport matrix. This matrix should be able to describe the equation of motion of the identified ions under the action of the dipole and quadrupole fields, such as to reproduce the measured final phase space parameters. The transport matrix is constructed based on differential algebraic methods which are implemented in the COSY INFINITY code [39]. By feeding as an input in the code a detailed description of the experimental conditions like the geometry of the two magnets, the measured values for the quadrupole and dipole fields, the acceptance of the spectrometer and the geometry of the FPD, the direct transport matrix is determined. Subsequently, the obtained matrix is fed as an input to a kinematics simulation algorithm. Starting from the randomly generated momentum

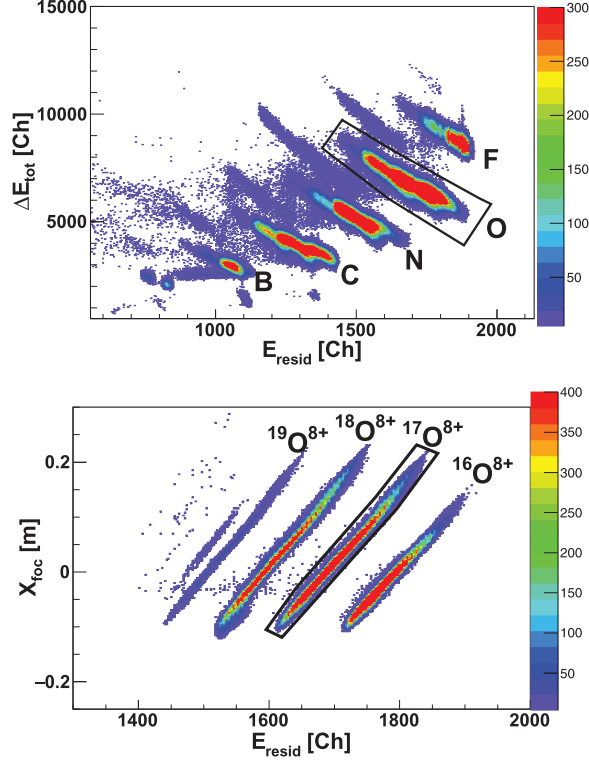


Fig. 1. – Typical identification plots for the $^{48}\text{Ti}(^{18}\text{O}, ^{17}\text{O})^{49}\text{Ti}$ reaction measured at 275 MeV. Top: $\Delta E_{\text{tot}} - E_{\text{resid}}$ correlation plot between the ions energy loss inside the gas tracker, ΔE_{tot} , and the residual energy, E_{resid} , measured by one silicon detector of the FPD. The various ion species are well-separated. A graphical selection on the contour of the oxygen ion events is depicted by the solid black line. Bottom: horizontal position at the MAGNEX focal plane, X_{foc} , as a function of the residual energy, after imposing the graphical condition on the oxygen contour as demonstrated in the top panel. The different loci correspond to ions with different ratio \sqrt{m}/q . A graphical selection on the $^{17}\text{O}^{8+}$ events is depicted by the solid black line.

vector at the target position, the ions path through the spectrometer is simulated up to the FPD and the simulated final phase space parameters $(x_f, \theta_f, y_f, \phi_f)$ are obtained. By comparing the simulated parameters to the measured ones, the validity of the direct transport matrix is evaluated. An example of such a comparison is demonstrated in fig. 2 for the one-proton transfer reaction. It is apparent that the simulated data reproduce adequately-well the experimental ones, proving the validity of the transport matrix. Subsequently, this matrix was inverted, then applied to measured final phase space parameters, so the momentum vector at the target position was reconstructed.

3.1. The $^{48}\text{Ti}(^{18}\text{O}, ^{19}\text{F})^{47}\text{Sc}$ reaction. – The reconstructed excitation energy spectrum, E_x , obtained with the $\text{TiO}_2 + ^{27}\text{Al}$ target is shown in fig. 3. The excitation energy was obtained from the missing mass method [32] as

$$(1) \quad E_x = Q_0 - Q,$$

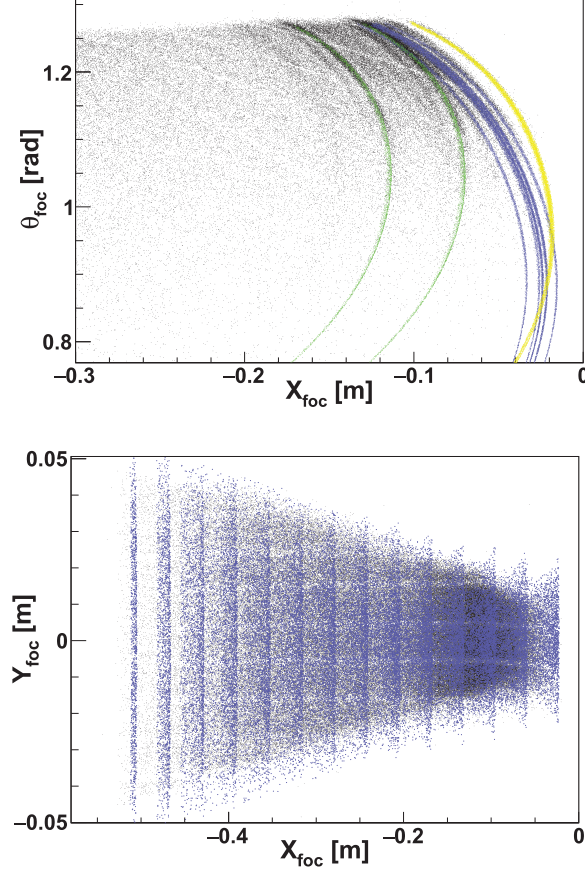


Fig. 2. – Top panel: the identified $^{19}\text{F}^{9+}$ ions from the data set obtained with the $\text{TiO}_2 + ^{27}\text{Al}$ target, shown by the black points, are compared to the simulated ones which are depicted with the coloured points in the $\theta_{\text{foc}} - X_{\text{foc}}$ representation [40]. For reasons of clarity, only few selective transitions corresponding to the one-proton transfer reaction on ^{48}Ti , ^{16}O and ^{27}Al were simulated and are presented with violet, green and yellow points, respectively. Bottom: same as in the figure on the top panel but for the data plotted in the $Y_{\text{foc}} - X_{\text{foc}}$ representation. For reasons of clarity, the experimental data are compared solely to the simulated ones corresponding to the $^{48}\text{Ti}(^{18}\text{O}, ^{19}\text{F})^{47}\text{Sc}$ reaction but considering transitions to a variety of excited states.

where Q_0 is the Q -value of the $^{48}\text{Ti}(^{18}\text{O}, ^{19}\text{F})^{47}\text{Sc}$ reaction, calculated considering that all nuclei at the entrance and exit channels are in their ground state (ground state (g.s.) to g.s. Q -value). The Q -value contains the masses of the nuclei at the entrance and exit channels, and the reconstructed kinetic energy and angle of the ^{19}F ions. In the same figure, contributions from the background due to the presence of the two contaminants in the target, appropriately normalized, are also shown. The background spectra were subtracted from the total one and the excitation energy spectrum for the $^{48}\text{Ti}(^{18}\text{O}, ^{19}\text{F})^{47}\text{Sc}$ reaction was obtained. Due to the high level density of the populated ^{47}Sc nucleus and the finite energy resolution (≈ 500 keV in full width at half maximum), transitions to isolated states of ^{19}F or ^{47}Sc nuclei were not observed. Therefore, the experimental yields were integrated in a wide energy range between $0 < E_x < 3.5$ MeV including thus the

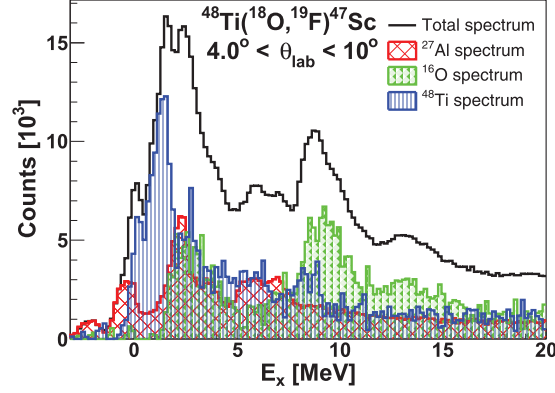


Fig. 3. – Decomposition of the excitation energy spectrum for the one-proton transfer reaction obtained in the data set with the $\text{TiO}_2 + {}^{27}\text{Al}$ target. The total spectrum is illustrated with the solid black line. The red-hatched area corresponds to the normalized background originating from the one-proton transfer reaction on the ${}^{27}\text{Al}$ backing, while the dotted green area corresponds to the background arising from oxygen component of the target. The blue-vertically-hatched area is the obtained excitation energy spectrum for the ${}^{48}\text{Ti}({}^{18}\text{O}, {}^{19}\text{F}){}^{47}\text{Sc}$ reaction, after subtracting the background contributions. Figure taken from ref. [30].

contribution of various excited states of ${}^{19}\text{F}$ and ${}^{47}\text{Sc}$ nuclei. The absolute differential cross-sections were determined after correcting the experimental yields for the overall efficiency of MAGNEX spectrometer [41] and the obtained angular distribution is presented in fig. 4. Since the angular range covered in the present measurement corresponds mainly to the so-called “dark” region after the grazing angle ($\theta_{gr}^{c.m.} = 7.6^\circ$), the angular distribution presents the typical exponential decrease associated to the strong absorption manifested after the grazing angle. The error in the data points includes the contribution from the statistical and the background subtraction uncertainties.

The angular distribution data were analyzed under the DWBA and CCBA frameworks using the FRESKO code [42]. In both calculations, the distorted waves at the entrance

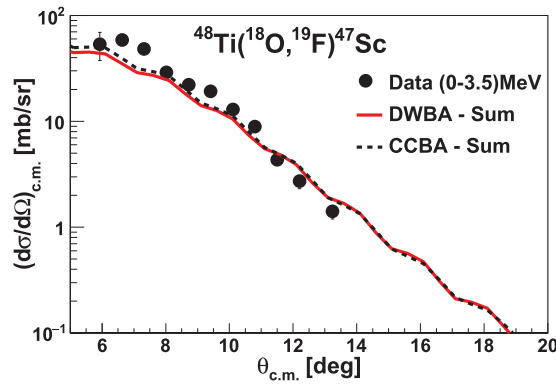


Fig. 4. – Present angular distribution data for the ${}^{48}\text{Ti}({}^{18}\text{O}, {}^{19}\text{F}){}^{47}\text{Sc}$ reaction, denoted with the black markers, are compared to the results of a DWBA and a CCBA calculation which are denoted with the solid red and dotted black lines, respectively. Figure taken from ref. [30].

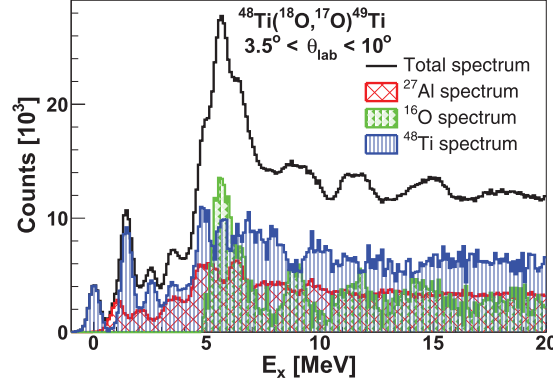


Fig. 5. – Preliminary analysis of the excitation energy spectrum for the one-neutron transfer reaction obtained in the data set with the $\text{TiO}_2 + ^{27}\text{Al}$ target. The total spectrum is illustrated with the solid black line. The red-hatched area corresponds to the normalized background originating from the one-neutron transfer reaction on the ^{27}Al backing, while the dotted green area corresponds to the background arising from oxygen component of the target. The blue-vertically-hatched area is the obtained excitation energy spectrum for the $^{48}\text{Ti}(^{18}\text{O}, ^{17}\text{O})^{49}\text{Ti}$ reaction, after subtracting the background contributions.

and exit channels were generated adopting the SPP for both the real and imaginary parts of the OPs, while the spectroscopic amplitudes were derived from large-scale shell model calculations using the KSHELL code [43]. For the calculation of the spectroscopic amplitudes corresponding to the projectile and target overlaps the p-sd-mod [44] and the SDPF-MU [45] interactions were invoked, respectively. The complete description of the adopted reaction models can be found in ref. [30]. The theoretical angular distributions are compared to the experimental data in fig. 4. It is apparent that both calculations are in very good agreement with the experimental data, suggesting the validity of the adopted optical potentials for the description of the elastic scattering at the entrance and exit channels and also confirming the shell-model description of the involved nuclei within the adopted model space.

3.2. The $^{48}\text{Ti}(^{18}\text{O}, ^{17}\text{O})^{49}\text{Ti}$ reaction. – The large acceptance in momentum of the MAGNEX spectrometer allowed the measurement of the one-neutron stripping reaction simultaneously with the one-proton transfer one using a unique set of magnetic fields. Following a similar procedure as the one described above, after the identification of the $^{17}\text{O}^{8+}$ ions (see fig. 1) a software ray reconstruction was applied to the data and the excitation energy was determined using eq. (1) with Q_0 being the g.s. to g.s. Q-value for the $^{48}\text{Ti}(^{18}\text{O}, ^{17}\text{O})^{49}\text{Ti}$ reaction. A preliminary analysis of the resulted excitation energy spectrum is shown in fig. 5. Once more, due to the presence of the aluminum backing and oxygen in the titanium target, a background subtraction procedure was performed in order to isolate the spectrum corresponding to ^{17}O and ^{49}Ti nuclei. In the final spectrum, several structures are well-pronounced associated to the populated states of ^{17}O and ^{49}Ti nuclei. The first structure is an isolated peak and corresponds to the g.s. to g.s. transition, while the rest of the observed structures include contributions from transitions to various states of both the ejectile and recoil nuclei. After the excitation energy of ≈ 8 MeV a rather constant evolution of the spectrum is observed to be compatible with the continuum background above the neutron emission threshold of ^{49}Ti nucleus. A

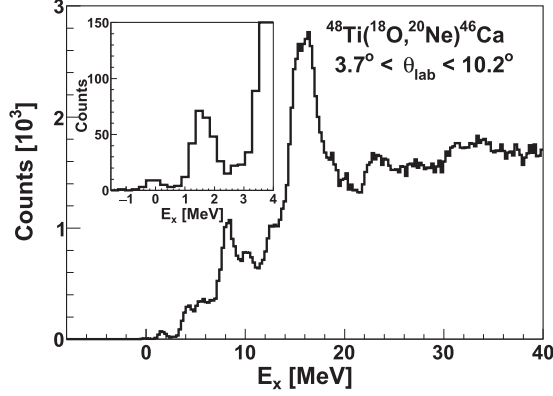


Fig. 6. – Preliminary reconstruction of data corresponding to the $^{48}\text{Ti}(^{18}\text{O}, ^{20}\text{Ne})^{46}\text{Ca}$ reaction at 275 MeV. In the inset a zoomed view at the first 4 MeV of the excitation energy spectrum is shown.

preliminary analysis of the energy spectra and the determination of angular distribution cross-sections has been performed as part of a Master Thesis and the results are reported elsewhere [46]. The theoretical interpretation of the data within the DWBA and CCBA frameworks is at an advanced stage and it will be the subject of a forthcoming publication of the NUMEN Collaboration.

3.3. The $^{48}\text{Ti}(^{18}\text{O}, ^{20}\text{Ne})^{46}\text{Ca}$ reaction. – In the same experiment, the two-proton transfer reaction was also measured, but in a separate run with different magnetic settings than those used for the measurement of one-nucleon transfer channels. The magnetic fields of the dipole bending magnet and the quadrupole were fixed according to the kinematics of the $^{48}\text{Ti}(^{18}\text{O}, ^{20}\text{Ne})^{46}\text{Ca}$ reaction ensuring that the $^{20}\text{Ne}^{10+}$ ejectiles corresponding to the g.s. to g.s. transition are transported at the center of the FPD. Considering the large momentum acceptance of MAGNEX, an excitation energy spectrum of ^{46}Ca up to $E_x \approx 56$ MeV was explored. A preliminary software trajectory reconstruction was applied to the data and the resulted excitation energy spectrum is presented in fig. 6. In the same figure, an inset was used in order to emphasize the region of the first low-lying states of the ejectile and recoil nuclei. Up to the excitation energy of $E_x \approx 4$ MeV, the observed structures are the fingerprints of the $^{48}\text{Ti}(^{18}\text{O}, ^{20}\text{Ne})^{46}\text{Ca}$ reaction. Beyond that energy, background contaminations originating from two-proton transfer on ^{27}Al and ^{16}O are present and thus should be subtracted from the total spectrum. The background subtraction procedure for this specific reaction as well as the determination of angular distribution cross-sections is in progress. Upon completion of the data reduction, the experimental cross-sections will be analyzed under the proper reaction frameworks as done previously in refs. [18, 19], in order to probe coupling channel effects as well as to quantify the contribution of simultaneous and sequential nucleon transfer in the measured two-proton transfer cross-sections.

4. – Conclusions

One- and two-nucleon transfer reactions for the system $^{18}\text{O} + ^{48}\text{Ti}$ at 275 MeV were measured at INFN-LNS as part of a global study which is performed under the NUMEN and NURE experimental campaigns. The various reaction ejectiles were detected

by the MAGNEX magnetic spectrometer in the angular regime between 3° and 15° in the laboratory reference frame. The analysis of the one-proton transfer reaction has been recently completed, while the analyses of the one-neutron and two-proton transfer reactions are at an advanced stage. The study of the one-neutron transfer reaction is complementary to the one-proton transfer one, since together they will clarify the degree of competition between sequential nucleon transfer and the direct single charge exchange mechanism, which in turn is a competitive process to the direct DCE mechanism. On the other hand, the study of two-proton and two-neutron transfer reactions will provide the appropriate constraints on the DCE mechanism in the $^{18}\text{O} \rightarrow ^{18}\text{Ne}$ transition. This work highlights the importance of studying not only the DCE reaction, but also all the competing channels that may populate the same final nuclear states.

* * *

The author would like to acknowledge financial support from the European Research Council (ERC) under the European Unions Horizon 2020 Research and Innovation Programme (Grant Agreement No. 714625).

REFERENCES

- [1] GANDO A. *et al.*, *Phys. Rev. Lett.*, **117** (2016) 082503.
- [2] ARNOLD R. *et al.*, *Phys. Rev. D*, **93** (2016) 112008.
- [3] ADAMS D. Q. *et al.*, *Phys. Rev. Lett.*, **124** (2020) 122501.
- [4] AGOSTINI M. *et al.*, *Phys. Rev. Lett.*, **125** (2020) 252502.
- [5] TETSUNO K. *et al.*, *J. Phys.: Conf. Ser.*, **1468** (2020) 012132.
- [6] CAPPUZZELLO F. *et al.*, *Eur. Phys. J. A*, **54** (2018) 72.
- [7] CAPPUZZELLO F. *et al.*, *Int. J. Mod. Phys. A*, **36** (2021) 2130018.
- [8] IWATA Y. *et al.*, *Phys. Rev. Lett.*, **116** (2016) 112502.
- [9] BELLEY A. *et al.*, *Phys. Rev. Lett.*, **126** (2021) 042502.
- [10] SANTOPINTO E. *et al.*, *Phys. Rev. C*, **98** (2018) 061601(R).
- [11] LENSKE H. *et al.*, *Prog. Part. Nucl. Phys.*, **109** (2019) 103716.
- [12] SHIMIZU N. *et al.*, *Phys. Rev. Lett.*, **120** (2018) 142502.
- [13] FERREIRA J. L. *et al.*, submitted to *Phys. Rev. C*.
- [14] BELLONE J. I. *et al.*, *Phys. Lett. B*, **807** (2020) 135528.
- [15] LAY J. A. *et al.*, *J. Phys.: Conf. Ser.*, **1056** (2018) 012029.
- [16] CAPPUZZELLO F. *et al.*, *Eur. Phys. J. A*, **51** (2015) 145.
- [17] SOUKERAS V. *et al.*, *Res. Phys.*, **28** (2021) 104691.
- [18] CARBONE D. *et al.*, *Phys. Rev. C*, **102** (2020) 044606.
- [19] FERREIRA J. L. *et al.*, *Phys. Rev. C*, **103** (2021) 054604.
- [20] CAVALLARO M. *et al.*, *Front. Astron. Space Sci.*, **8** (2021) 659815.
- [21] CALABRESE S. *et al.*, *Phys. Rev. C*, **104** (2021) 064609.
- [22] BROGLIA R. A. *et al.*, in *Advances in Nuclear Physics*, edited by BARANGER M. and VOGT E., Vol. **6** (Plenum Press, New York) 1973, pp. 287–457.
- [23] TIMOFEYUK H. *et al.*, *Prog. Part. Nucl. Phys.*, **111** (2019) 103738.
- [24] ASCUITTO R. J. *et al.*, *Phys. Rev.*, **181** (1969) 1396.
- [25] CANDITO RIBEIRO M. A. *et al.*, *Phys. Rev. Lett.*, **78** (1997) 3270.
- [26] SPATAFORA A. *et al.*, *Phys. Rev. C*, **100** (2019) 034620.
- [27] CARBONE D. *et al.*, *Universe*, **07** (2021) 58.
- [28] LA FAUCI L. *et al.*, *Phys. Rev. C*, **104** (2021) 054610.
- [29] CAVALLARO M. *et al.*, *PoS, BORMIO2017* (2017) 015.
- [30] SGOUROS O. *et al.*, *Phys. Rev. C*, **104** (2021) 034617.
- [31] BRISCHETTO G. A., these proceedings.
- [32] CAPPUZZELLO F. *et al.*, *Eur. Phys. J. A*, **52** (2016) 167.

- [33] PAKOU A. *et al.*, *Eur. Phys. J. A*, **57** (2021) 25.
- [34] KOULOURIS S. *et al.*, *EPJ Web of Conferences*, **252** (2021) 07005.
- [35] SOULIOTIS G. A. *et al.*, *Nucl. Instrum. Methods Phys. Res. A*, **1031** (2022) 166588.
- [36] TORRESI D. *et al.*, *Nucl. Instrum. Methods Phys. Res. A*, **989** (2021) 164918.
- [37] CAPPUZZELLO F. *et al.*, *Nucl. Instrum. Methods Phys. Res. A*, **621** (2010) 419.
- [38] CAPPUZZELLO F. *et al.*, *Nucl. Instrum. Methods Phys. Res. A*, **638** (2011) 74.
- [39] MAKINO K. *et al.*, *Nucl. Instrum. Methods Phys. Res. A*, **427** (1999) 338.
- [40] SGOUROS O. *et al.*, *EPJ Web of Conferences*, **252** (2021) 04002.
- [41] CAVALLARO M. *et al.*, *Nucl. Instrum. Methods Phys. Res. A*, **637** (2011) 77.
- [42] THOMPSON I. J., *Comput. Phys. Rep.*, **7** (1988) 167.
- [43] SHIMIZU N. *et al.*, *Comput. Phys. Commun.*, **244** (2019) 372.
- [44] UTSUNO Y. *et al.*, *Phys. Rev. C*, **83** (2011) 021301(R).
- [45] UTSUNO Y. *et al.*, *Phys. Rev. C*, **86** (2012) 051301(R).
- [46] CUTULI M., *Study of the $^{48}\text{Ti}(^{18}\text{O}, ^{17}\text{O})^{49}\text{Ti}$ one-neutron transfer reaction at 275 MeV in the context of the NUMEN project*, Master Thesis, University of Catania (2021).